Article

Synthesis and Characterization of Mono- and Biphasic Ca1−xMnxHPO4·nH2O Compounds

Mohammed Alyami , Haya Ali Alsunaidi , Juma'a Al-Kafawein , Abdulaziz A. Alanazi , Satam Alotibi , Fahad Abdulaziz , Nada T. Mahmoud , Mazen Alshaaer *

Posted Date: 29 August 2024

doi: 10.20944/preprints202408.2123.v1

Keywords: CaHPO4·2H2O; MnHPO4·(H2O)3; unit cell; SEM; crystal structure

Article

Synthesis and Characterization of Mono- and Biphasic $Ca_{1-x}Mn_xHPO_4{\cdot}nH_2O$ Compounds for Biomedical Applications

Mohammed Alyami [1], Haya Ali Alsunaidi [1], Juma'a Al-Kafawein [2], Abdulaziz A. Alanazi [3], Satam Alotibi [1], Fahad Abdulaziz [4], Nada T. Mahmoud [5] and Mazen Alshaaer [1,6,*]

[1] Department of Physics, College of Science and Humanities in Al-Kharj, Prince Sattam bin Abdulaziz University, Al-Kharj 11942, Saudi Arabia
[2] Department of Chemistry, King Faisal University, Al-Hassa 31982, Saudi Arabia
[3] Department of Chemistry, College of Science and Humanities in Al-Kharj, Prince Sattam bin Abdulaziz University, Al-Kharj 11942, Saudi Arabia
[4] Department of Chemistry, College of Science, University of Ha'il, Ha'il 81451, Saudi Arabia
[5] Physics Department, The University of Jordan, Amman 11942, Jordan
[6] Department Mechanics of Materials and Constructions (MEMC), Vrije Universiteit Brussels (VUB), Pleinlaan 2, 1050 Brussels, Belgium
* Correspondence: mazen.alshaaer@vub.be

Abstract: Calcium phosphates and manganese phosphates play a significant role in biomedical and engineering applications, and these compounds are both synergistic. These compounds could have great potential for use in different applications, particularly as precursors of biomaterials. Therefore, the aim of this study was to explore the effect of the gradual replacement of Ca^{2+} with Mn^{2+} on the phase composition and crystal structure of brushite ($CaHPO_4{\cdot}2H_2O$), which could be useful for the production of Mono- and Biphasic $Ca_{1-x}Mn_xHPO_4{\cdot}nH_2O$ Compounds. In order to prepare the starting solutions required for this study, $Ca(NO_3)_2{\cdot}4H_2O$, $(NH_4)_2HPO_4$, and $Mn(NO_3)_2{\cdot}4H_2O$ were used at various molar concentrations. Afterwards, the $Ca_{1-x}Mn_xHPO_4{\cdot}nH_2O$ compounds were prepared using dissolution and precipitation methods. These compounds were characterized using XRD, SEM, FT-IR, XPS, and TGA techniques. The findings revealed that Mn substituted Ca partially at low Mn/Ca molar ratios, 0.25, and Mn doping increased the unit cell of $CaHPO_4{\cdot}2H_2O$. The produced biphasic compound was composed of monoclinic $CaHPO_4{\cdot}2H_2O$ and nanostructured orthorhombic $MnHPO_4{\cdot}(H_2O)_3$ after a continuous increase in the Mn/Ca molar ratio to 1.5. When the Ca/Mn molar ratio was above 1.5, a monophasic compound of the $MnHPO_4{\cdot}(H_2O)_3$ phase was formed. The $MnHPO_4{\cdot}(H_2O)_3$ compound was successfully prepared for the first time using this dissolution-precipitation method. It was also established that the Mn/Ca ratio of the starting solution can be modified to produce $CaHPO_4{\cdot}2H_2O$ and $MnHPO_4{\cdot}(H_2O)_3$ phases with specific weight percent compositions.

Keywords: $CaHPO_4{\cdot}2H_2O$; $MnHPO_4{\cdot}(H_2O)_3$; unit cell; SEM; crystal structure

1. Introduction

To address various bone defects in the body that are caused by osteoporosis, surgeries, or fractures, improved bone substitutes and implants are frequently requested. Autologous tissue is usually used for bone resorption [1,2]. However, conventional bone substitutes and implants come with challenges, including high rates of infection and limited graft materials. The limited number of donors and safety concerns make bone marrow treatments challenging [3,4]. Implant-related infections have a significant impact on clinical and socioeconomic outcomes [5,6]. Host defenses and antimicrobial treatments are less effective than usual, due to the formation of a bacterial biofilm on inert surfaces and nearby tissues. More surgeries, longer hospital stays, and a higher risk of death are caused by current treatments that involve surgery, antibiotics, and even implant removal [7–9]. Synthetic bone materials have emerged as a more reliable replacement for autografts to address these

 doi:10.20944/preprints202408.2123.v1

issues, which has led to a decrease in infection risks and complications. Implants that can degrade naturally in the body are becoming more necessary, due to their clinical viability.

Biodegradable materials are an important and promising choice as substitutes for bones. This is because they can be absorbed over time and replaced with natural bone tissue, resulting in a reduction in the need for further surgeries. Biodegradable materials possess inductive, osteogenic, and conductive characteristics. The use of biodegradable materials for bone regeneration is hindered by the difficulty of integrating and vascularizing them within the body [10,11]. Calcium phosphate (CaP) is utilized in many fields, including biology, medicine, environmental science, and engineering, due to its structural characteristics [12]. In medical applications, CaPs are advantageous as they are highly bioactive, have low toxicity, and exhibit a high similarity to bone minerals [1,4]. Advanced biocements and bioceramics for dental and medical purposes are currently being developed using CaPs [10,13].

Acidic and alkaline supersaturated solutions produce a range of CaP precipitates. The major common CaP phases are hydroxyapatite (HA), octacalcium phosphate (OCP), monetite (DCPA), β-tricalcium phosphate (β-TCP), brushite (DCPD) [14,15], and amorphous calcium phosphate (ACP). These phases have different solubilities and crystalline structures. The spontaneous formation of calcium phosphate phases in aqueous supersaturated solutions can be facilitated using seeded crystal growth or substrate assistance [4–16]. $CaHPO_4{\cdot}2H_2O$, also referred to as brushite, is necessary for bioceramics, bone cement, and HA [11,17]. A pH level of around 7.4 enables the body to reabsorb it, facilitating bone tissue re-modeling, and its stability is preserved at temperatures lower than 60 °C with pH levels that vary from 4 to 6.5 [18].

Brushite ($CaHPO_4{\cdot}2H_2O$) is the precursor to other CaP phases, including HA and OCP. The monoclinic mineral (space group Ia) exhibits lattice parameters that range from a to 5.81, b to 15.18, c to 6.24, and β to 116.42°. It has a structure with layers, with $CaHPO_4$ sheets that have corrugated surfaces and two water molecules that alternate in the direction [010]. The representation of each Ca^{2+} ion in the octahedral is surrounded by six oxygen phosphate molecules from four phosphorous groups $(HPO_4)^{2-}$ and two oxygens from two H_2O molecules [19]. The characteristic features of the brushite mineral, such as its biocompatibility, high adsorption capacity, and high porosity, make it a suitable choice for various medical applications.

The present investigation was devoted to altering metals (i.e., manganese ions) in the calcium phosphate framework. Metal ions can be used to produce biomaterials with better mechanical characteristics and acceptable setting times [14]. The incorporation of metals into biomaterials can lead to significant control over the cell density. This method has led to the successful development of regenerative medicine. This examination focused on metal substitutions and their impact on the chemical and physical properties of biocides, including the setting time, mechanical properties, microstructure, ion release, and injectability [8,20]. Metal-doped calcium phosphates provide benefits such as osteogenesis, antibacterial properties, and angiogenesis, as well as potential utility as drug carriers. Manganese has an impact on bone metabolism, and calcium phosphates doped with manganese have been observed to stimulate osteoblast growth and differentiation [21]. Furthermore, abnormalities in bone thickness and length were shown to increase with Mn deficiency [22]. Brushite can only be achieved in a single phase with a Mn substitution of less than 20% when the starting solutions contain more than 20% Mn ions. In the case of Mn^{2+}, brushite can be formed as a single crystalline phase up to 20%, whereas the pattern of brushite with 25% manganese atoms also contains a secondary phase, $(Mn)_3(PO_4)_2{\cdot}7H_2O$), and an amorphous phase that becomes predominant with a 30% calcium substitution by manganese [22].

Calcium phosphates such as brushite and manganese phosphates play a significant role in biomedical applications, and these substances are both synergistic [23,24]. The Mn content in these compounds must be carefully considered to avoid any adverse effects. The development of bone substitutes and implants necessitates a balance between factors such as bioactivity, osteogenic properties, biocompatibility, and antimicrobial activities. Calcium phosphate dihydrate (DCPD or brushite) materials are promising candidates for bone regeneration due to their biocompatibility and resemblance to natural bone tissue. CaP materials that include antimicrobial compounds such as Mn^{+}

 doi:10.20944/preprints202408.2123.v1

can be used to prevent implant-related infections [22–24]. To prevent negative consequences, it is important to carefully control the concentration of Mn ions.

As stated above, there have been no comprehensive investigations into the consequences of a gradual Mn substitution/replacement for Ca ions from 0% to 100% in DCPD (brushite). The only investigation that has been conducted was on the effect of doping brushite with a manganese ion percentage of less than 30%. The synthesis of compounds with both manganese phosphates and calcium phosphates in specific ratios is impossible, although the ability to combine both phases in biomedical applications is of high importance. The preparation of these phases is typically undertaken separately before they are combined. The impact of replacing Ca ions in brushite with Mn ions entirely at a full scale is what makes this research work innovative. Therefore, investigations were conducted to determine the thermal properties, phase composition, and crystal morphology of the compounds produced at different levels of ion substitution. This research addresses a significant research gap and may be valuable for basic compound synthesis to create novel (Mn and Ca) phosphate-based precursors of biomaterials with distinct antibacterial activities and high bioactivity. Many other applications in bone tissue engineering and pharmaceutical industries, such as bone cement and bioceramic synthesis, are highly promising due to the use of synthesized products and minerals.

2. Materials and Methods

2.1. Materials and Chemicals

The source of phosphorous ions was diammonium hydrogen phosphate, $(NH_4)_2HPO_4$ (Techno Pharmchem, Delhi, India). Manganese (II) nitrate tetrahydrate ($Mn(NO_3)_2{\cdot}4H_2O$) and calcium nitrate tetrahydrate ($Ca(NO_3)_2{\cdot}4H_2O$) were purchased from LOBA Chemie in Mumbai, India. The PURELAB option-Q purification system from ELGA in the UK was used to obtain distilled water with a low conductivity of 0.06 μS/cm. An ISOTEMP magnetic stirrer from Fisher Scientific in China was used to prepare the solutions, and the weights were recorded using a digital analytical balance (OHAUS, Parsippany, NJ, USA).

2.2. Synthesis of $Ca_{1-x}Mn_xHPO_4{\cdot}nH_2O$ Compounds

The synthesis procedures and the compositions of seven different $CaxMn_{1-x}HPO_4{\cdot}nH_2O$ compounds using solutions of $(NH_4){\cdot}2HPO_4$, $Ca(NO_3)_2{\cdot}4H_2O$, and $Mn(NO_3)_2{\cdot}4H_2O$ with specific molar ratios of P, Ca, and Mn ions are reported in Table 1.

The $Ca(NO_3)_2{\cdot}4H_2O$ solution and the $(NH4)_2HPO_4$ solution were mixed at a flow rate of around 2 mL/min to produce pure brushite (referred to as BMn0 in Table 1). To achieve a 1 Ca/P molar ratio, it took approximately one hour for the mixing process to be conducted using a glass funnel equipped with a stopcock and maintaining a stirring speed of 450 rpm. To ensure thorough mixing, the solution was stirred at RT for 60 minutes and ammonia was added. The pH level was maintained within the range of 6–6.5 through adding ammonia (15 moL/L; Labochemie, Mumbai, India). The resultant white precipitate was eluted with a Büchner funnel and qualitative filter paper with a thickness of 45 μm (Ø 12 cm, Double Rings, China). In order to prevent clumping, the filter cake was washed with deionized water and ethanol [18,25,26]. A watch glass (ED53/E2, Binder, Tuttlingen, Germany) was used to dry the sample in an oven set at 40 degrees Celsius for 7 days [27].

As shown in Table 1, the solutions for compounds BMn2, BMn4, BMn5, BMn6, and BMn10 were merged in the molar ratios specified. Following the same process as before, 100 mL of the end result was mixed with 100 mL of the $(NH_4)_2HPO_4$ solution at a flow rate of approximately 2 mL per minute. BMn10 was prepared by following the same method, but with $(NH_4)_2HPO_4$ and $Mn(NO_3)_2{\cdot}4H_2O$ mixed in.

 doi:10.20944/preprints202408.2123.v1

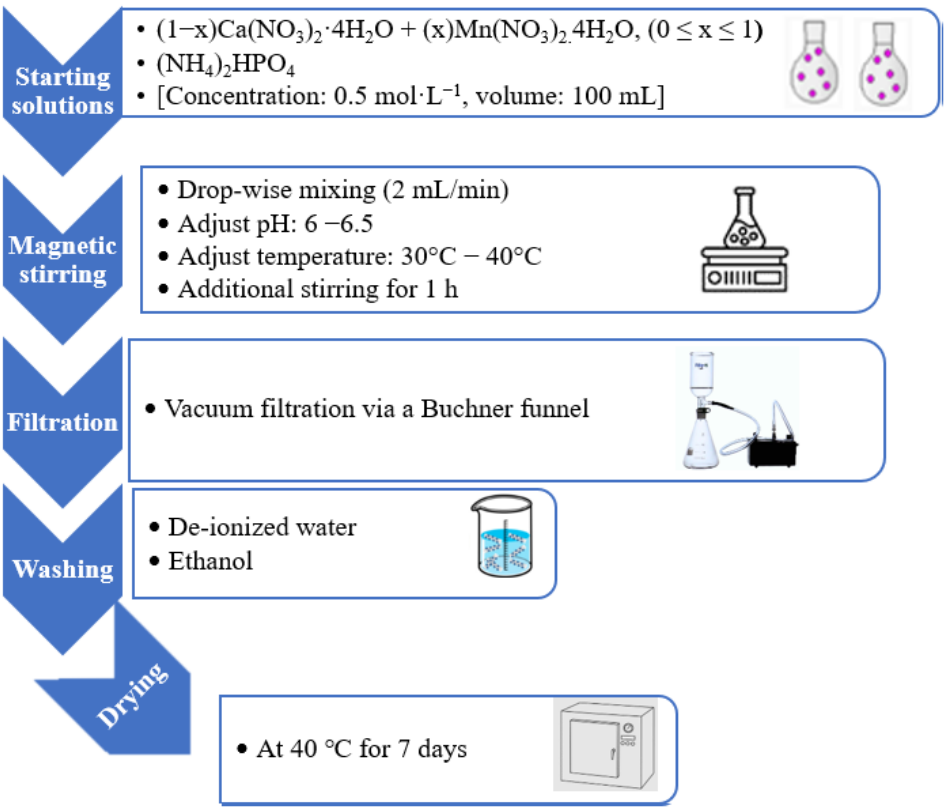

Figure 1. Experimental design for the preparation of the $Ca_{1-x}Mn_xHPO_4{\cdot}nH_2O$ compounds.

Table 1. Molar proportions of $(NH4)_2HPO_4$, $Ca(NO_3)2{\cdot}4H_2O$, and $Mn(NO_3)_2{\cdot}4H_2O$, in addition to the Mn/Ca molar ratios used for the preparation of $Ca_{1-x}Mn_xHPO_4{\cdot}nH_2O$ compounds.

ID	$(NH_4)_2HPO_4$	$Ca(NO_3)_2{\cdot}4H_2O$	$Mn(NO_3)_2{\cdot}4H_2O$	Mn/Ca Molar Ratio
BMn0	1	1	0	0
BMn2	1	0.8	0.2	0.25
BMn4	1	0.6	0.4	0.67
BMn5	1	0.5	0.5	1.0
BMn6	1	0.4	0.6	1.5
BMn8	1	0.2	0.8	4
BMn10	1	0	1	-

2.3. Characterization Techniques

A qualitative mineralogical analysis and phase composition of the BMn0–BMn10 samples was performed using an XRD diffractometer 6000, Shimadzu (Kyoto, Japan). To analyze the samples, a cobalt tube was used and the scans were carried out at a 2-theta range of 10° to 60°, with a scan rate of 2°/min. Crystal Impact—MATCH was used to process the powder XRD diffraction data for the crystal analysis and phase composition (software version 3.15, Bonn, Germany).

An Inspect F50 instrument (FEI Company, Eindhoven, the Netherlands) was utilized to obtain a comprehensive view of the product morphology.

The surface chemistry and the binding energy of the various compounds were measured and recorded using elemental XPS (X-ray photoelectron spectroscopy) (Thermo K-Alpha spectrometer, USA).

A Thermo Scientific Nicolet iS5 FT-IR spectrometer (USA) was utilized to detect molecular vibrations using IR light, and to obtain infrared spectra in the range of 4000 to 400 cm^{-1}.

The mass loss as a function of temperature from 40 °C up to 800 °C was determined using thermogravimetric analysis (TGA) (Germany, TG 209 F1 Libra). The temperature was increased at the rate of 4 °C/min under a helium atmosphere.

 doi:10.20944/preprints202408.2123.v1

3. Results and Discussion

3.1. Phase Characterization and Microstructural Analysis

Analysis of the X-ray diffraction scans of various powders, including monophasic compounds (BMn0, BMn2, BMn8, and BMn10), and biphasic powders (BMn4, BMn5, and BMn6) are presented in Figure 2. The XRD patterns revealed three major stages of $Ca_{1-x}Mn_xHPO_4{\cdot}nH_2O$ compounds. Monophasic $CaHPO_4{\cdot}2H_2O$ compounds (BMn1 and BMn2), Biphasic $CaHPO_4{\cdot}2H_2O$ - $MnHPO_4{\cdot}(H_2O)_3$ compounds (BMn4, BMN5, and BMn6), and finally monophasic $MnHPO_4{\cdot}(H_2O)_3$ compounds (BMn8 and BMn10).

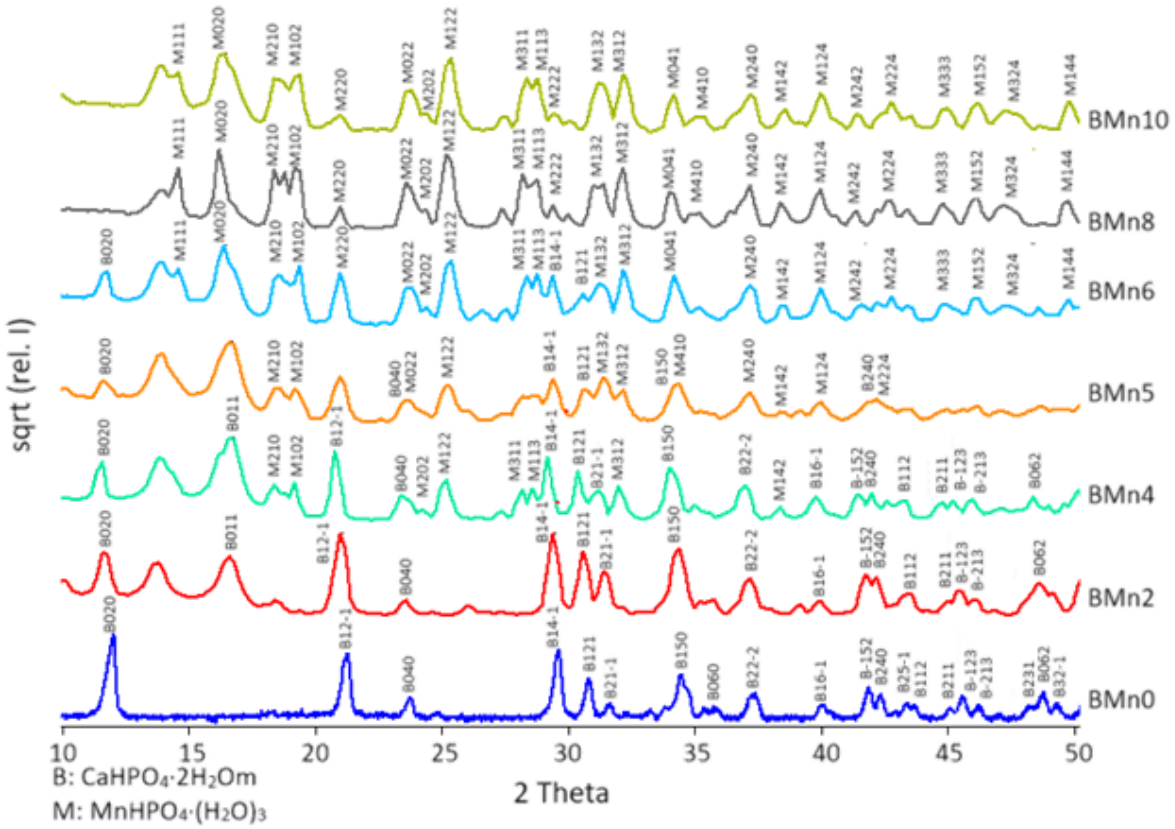

Figure 2. X-ray diffraction scans obtained from the $Ca_{1-x}Mn_xHPO_4{\cdot}nH_2O$ compounds that were produced in accordance with the conditions presented in Figure 1 and Table 1.

Pure $CaHPO_4{\cdot}2H_2O$ (BMn0) was confirmed to be formed when the solutions of $Ca(NO_3)2{\cdot}4H_2O$ and $(NH4)_2HPO_4$ were combined with an equal calcium-to-phosphorous molar ratio, as reported in Table 1. The major crystallographic planes corresponding to the Miller indices of $(14\bar{1})$, (020), and $(12\bar{1})$ were observed to display crystal expansion, which suggested a monoclinic structure. The significant crystal growth along the (020) plane was indicated by the XRD peak at a 2-theta of 11.8° [23]. Increasing the substitution of Ca by Mn to 20% (BMn2) did not cause any observable changes in the phase composition. A monophasic $CaHPO_4{\cdot}2H_2O$ is observed but with the appearance of new peak along the (011) plane alongside of intensity changes in the other peaks [28]. The appearance of an unidentified XRD peak associated with Mn contents, BMn2-BMn10, was observed at the 2-Theta of 14.08°.

The formation of the biphasic compounds of $CaHPO_4{\cdot}2H_2O$ and $MnHPO_4{\cdot}(H_2O)_3$ can is shown in the patterns of second stage (BMn4, BMn5, and BMn6). The new phase $MnHPO_4{\cdot}(H_2O)_3$, was represented by several peaks. It is possible to observe an increase in the intensity of peaks associated with $MnHPO_4{\cdot}(H_2O)_3$, (111), (210), (102), and(311) at the expense of the peaks associated with $CaHPO_4{\cdot}2H_2O$, (020), $(12\bar{1})$, and $(14\bar{1}$.

 doi:10.20944/preprints202408.2123.v1

In the third stage, when higher Mn/Ca molar ratios were present in the initial solutions, a monophasic powder of $MnHPO_4(H_2O)_3$ (Mn8 and Mn10) was produced. The many planes that were identified as being related to this phase are shown in Figure 2. This is a unique compound which is prepared by using this preparation dissolution – precipitation method for the first time [29].

To investigate the unit cell parameters and the phase composition in more detail, XRD scans and Rietveld refinement were used, where Table 2 shows the results of the software analysis. Figure 3 shows the change in the phase composition resulting from increasing the substitution of Ca by Mn in starting solutions. At this substitution stage, however, there is a clear increase in the size of the unit cell of $CaHPO_4.2H_2O$ from 485.72 **Å³** to 494.52 **Å³**, which confirms the substitution of Ca with Mn. Mn substitution up to 20% , BMn2, in this initial stage also led to a significant reduction in the Crystallite Size, Figure 4, from 9804 Å to 431 Å. The formation of the second phase, $MnHPO_4(H_2O)_3$, with Ca replacement with Mn of about 40%, BMn4, indicates that the limits of Mn substitution in $CaHPO_4.2H_2O$ range from 20% to 40%, which is consistent with previous studies [22].

Table 2. The phase composition and the lattice parameters of the $Ca_{1-x}Mn_xHPO_4{\cdot}nH_2O$ compounds.

	Phase Composition	% wt.	Crystal Structure	a(Å)	b (Å)	c(Å)	ß°	Unit Cell Volume (Å³)	Crystallite Size (nm) *
BMn0	$CaHPO_4.2H_2O$	100	Mono.	5.80	15.13	6.20	116.43	485.72	9804
BMn2	$CaHPO_4.2H_2O$	100	Mono.	5.81	15.20	6.25	116.41	494.52	305
BMn4	$CaHPO_4.2H_2O$	56	Mono	5.82	15.22	6.27	116.41	496.65	431
	$MnHPO_4(H_2O)_3$	44	Ortho	10.41	10.86	10.91	90	1152.33	117
BMn5	$CaHPO_4.2H_2O$	29	Mono.	5.81	15.21	6.26	116.41	496.65	181
	$MnHPO_4(H_2O)_3$	71	Ortho	10.41	10.86	10.19	90	1152.33	217
BMn6	$CaHPO_4.2H_2O$	19	Mono	5.81	15.19	6.24	116.41	493.43	321
	$MnHPO_4(H_2O)_3$	81	Ortho	10.41	10.86	10.19	90	1152.33	358
BMn8	$MnHPO_4(H_2O)_3$	100	Ortho	10.41	10.86	10.19	90	1152.01	477
BMn10	$MnHPO_4(H_2O)_3$	100	Ortho	10.41	10.86	10.19	90	1152.01	313

* Scherrer equation.

The increase in Mn ions from 40% (BMn4) up to 60% (BMn6) in the "starting" solutions (Table 1) corresponded to an increase in the content of $MnHPO_4(H_2O)_3$ at the expense of $CaHPO_4{\cdot}2H_2O$, Figure 3. Their respective standards were met by the lattice parameters, crystal structures, and unit cell volumes of both phases [29–31]. As the Mn/Ca molar ratio increased to 1.5, the unit cell volume of $CaHPO_4{\cdot}2H_2O$ retain its large size compared with pure $CaHPO_4{\cdot}2H_2O$, BMn0. The Mn ions were not just involved in $MnHPO_4(H_2O)_3$ precipitation, but they also became integrated in the $CaHPO_4{\cdot}2H_2O$ lattice as dopants or substitutes, as indicated by the variations in the unit cell volume (Table 2).

 doi:10.20944/preprints202408.2123.v1

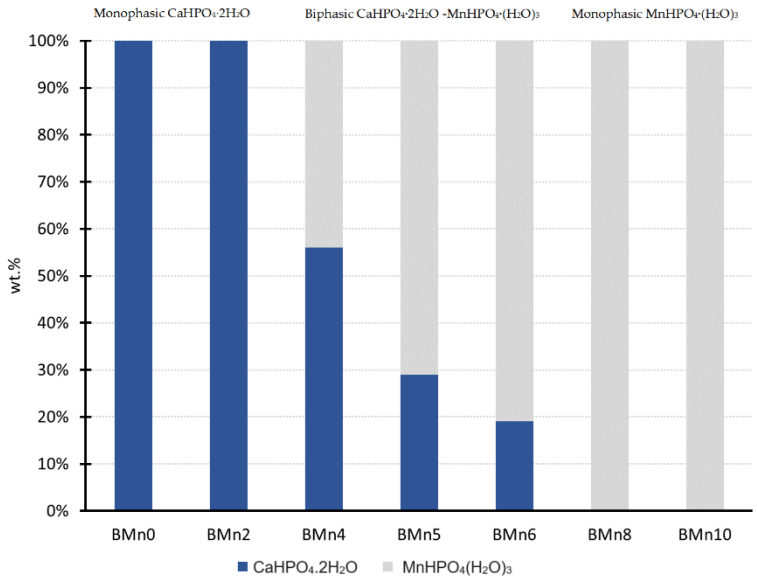

Figure 3. Phase composition of the produced compounds, $MnHPO_4(H_2O)_3$ and $CaHPO_4{\cdot}2H_2O$, compared with the Mn molar fraction in the starting solutions.

A rare crystal structure, $MnHPO_4(H_2O)_3$, precipitates spontaneously in aqueous solution when the Mn/Ca ratio exceeded 1.5, and it resulted in monophasic $MnHPO_4(H_2O)_3$ (BMn8 and BMn10). Similar XRD patterns of the BMn8 and BMn8 are illustrated in Figure 2. This rare phase, $MnHPO_4(H_2O)_3$, with high potential applications in biomedical applications and as catalyst, was prepared for the first time using this method. The substitution limit of Mn with Ca varies from 20% (BMn8) to 40% (BMn6), which is a similar ratio of Mn substitution in CaHPO4·2H2O, BMn2 and BMn4.

Figure 4 illustrates the changes in crystallite size of each compound, $MnHPO_4(H_2O)_3$ and $CaHPO_4{\cdot}2H_2O$, as a function of Mn contents. The crystallite size of $CaHPO_4{\cdot}2H_2O$ decreases sharply from 9804 Å to 431 Å because of doping by Mn, BMn2. The crystallite size of $MnHPO_4(H_2O)_3$ exhibits an increasing trend by increasing the Mn from 40%, BMn4, up to 80%, BMn. Unlike BMn2, when Mn substitutes decrease the crystal size of $CaHPO_4{\cdot}2H_2O$, Ca substitutes increase the crystal size of pure $MnHPO_4(H_2O)_3$, BMn8.

Figure 5 presents pure monophasic $CaHPO_4{\cdot}2H_2O$ (BMn0), as well as Mn doped $CaHPO_4{\cdot}2H_2O$, BMn2, biphasic compounds (BMn4, BMn5, and BMn6), and monophasic $MnHPO_4(H_2O)_3$ compounds (BMn8 and BMn10) with varied Mn/Ca molar ratios. The presence of monoclinic crystals of brushite (BMn0) with dimensions of $0.6 \times 6 \times 12\ \mu m^3$, Figure 5A, is in line with previous studies [19,32]. As the Mn/Ca ratio increased to 0.25, BMn2, the SEM images showed that the size of $CaHPO_4{\cdot}2H_2O$ decreases sharply to nanoscale, Figure 5B, which is in good agreement with the XRD analysis as reported in Table 2 and Figure 4. The nanostructured monoclinic $CaHPO_4{\cdot}2H_2O$ crystals are observed with Mn replacement of Ca by Mn up to 60%, BMn4, BMn5, and BMn6, as shown in Figures 5C, 5D, and 5 E respectively. In addition, these Figures show nanosized orthorhombic crystals of $MnHPO_4(H_2O)_3$ developed along with monoclinic CaHPO4·2H2O. Higher Mn/Ca molar ratios up to 4 led to an increase in the crystal size of $MnHPO_4(H_2O)_3$, Figure 5F. The crystal size of pure monophasic $MnHPO_4(H_2O)_3$ (BMn10), Figure 5G, is smaller than Ca-doped $MnHPO_4(H_2O)_3$ (BMn8), Figure 5F. The $MnHPO_4(H_2O)_3$ orthorhombic crystals in BMn6, BMn8, and BMn10 compounds are also illustrated in Figure 6A, 6B, and 6C respectively with higher magnification.

 doi:10.20944/preprints202408.2123.v1

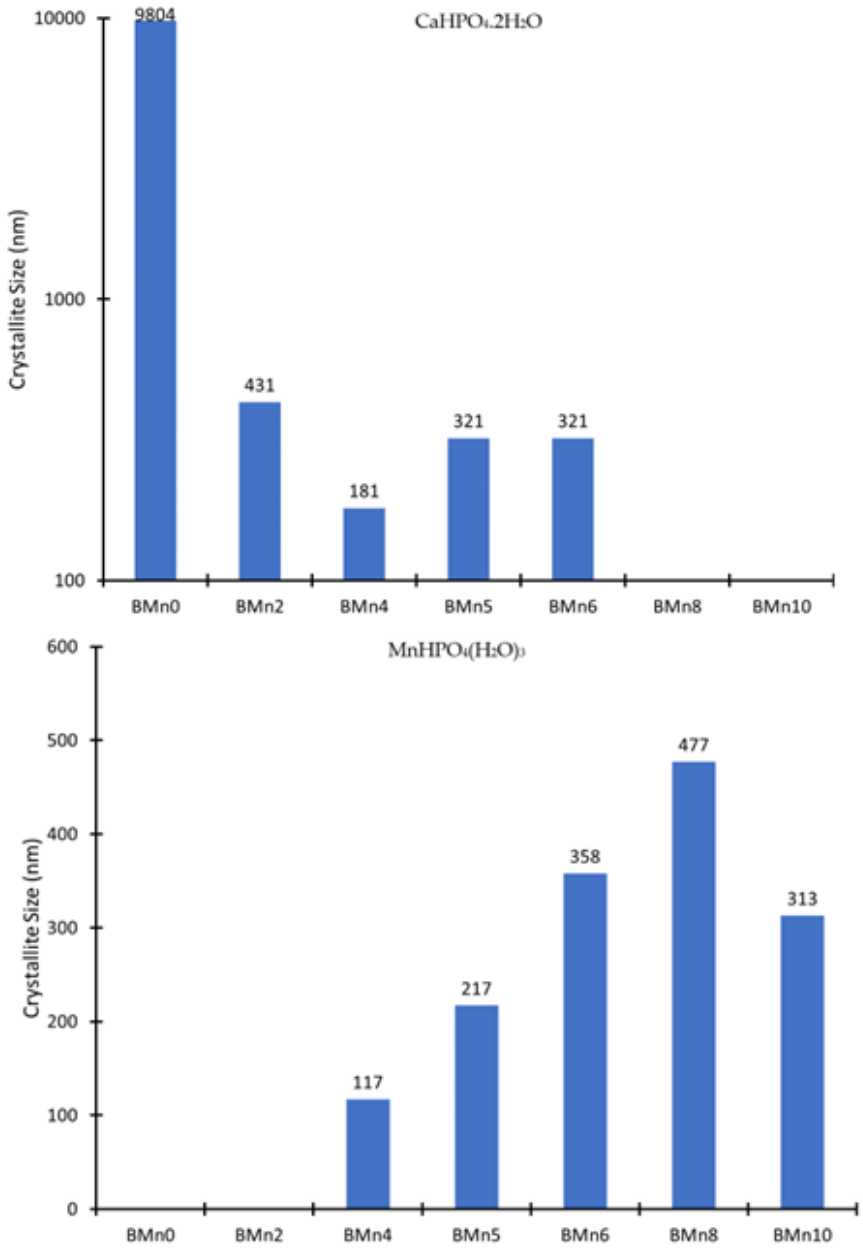

Figure 4. Crystallite sizes of the produced compounds: (up) $CaHPO_4{\cdot}2H_2O$ and (down) $MnHPO_4(H_2O)_3$ as a function of increasing Mn contents.

The SEM analysis verified the XRD data, indicating that $CaHPO_4{\cdot}2H_2O$ and $MnHPO_4(H2O)_3$ were present in the resulting compounds that replaced Ca ions with Mn ions (BMn4 to BMn6). The relationship between the $CaHPO_4{\cdot}2H_2O$ and $MnHPO_4(H_2O)_3$ proportions and the Mn content in the initial solutions was established using these results, which confirmed that Mn is involved in different stages of the reactions.

 doi:10.20944/preprints202408.2123.v1

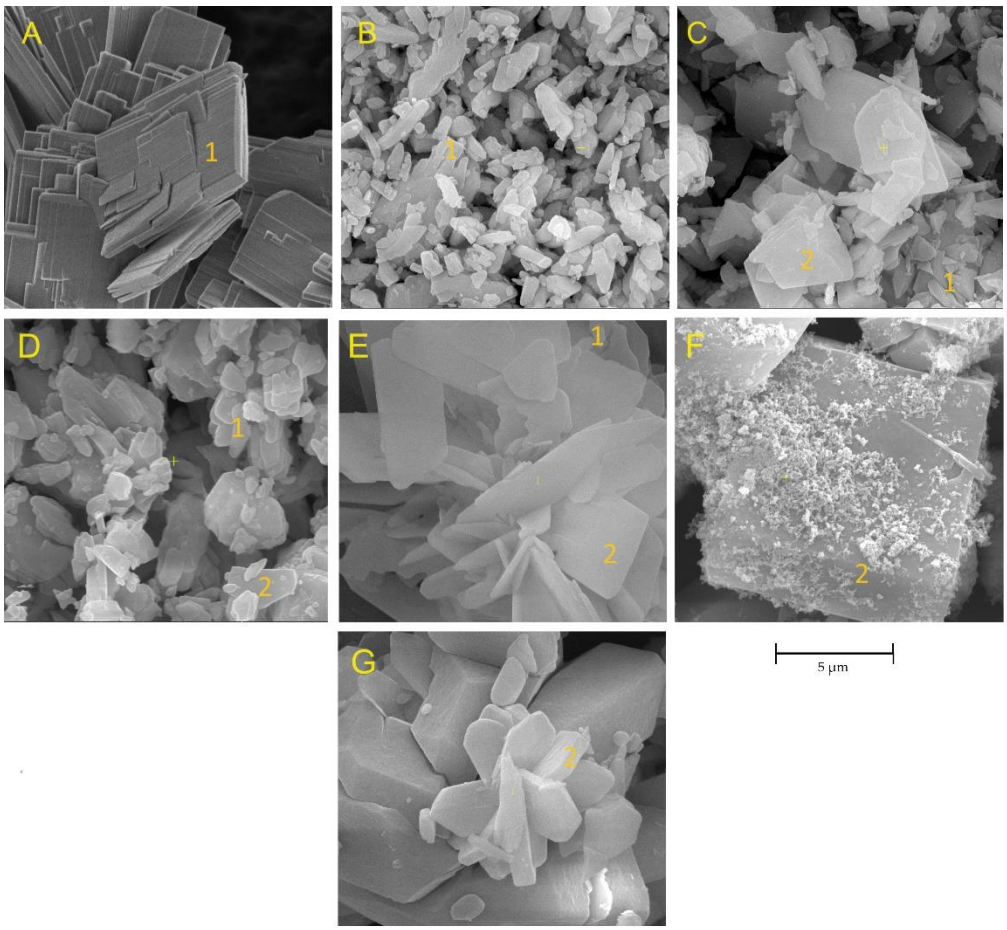

Figure 5. SEM images of the $Ca_{1-x}Mn_xHPO_4 \cdot nH_2O$ compounds as shown in Table 1: (A) BMn0, (B) BMn2, (C) BMn4, (D) BMn5, (E) BMn6, (F) BMn8, and (G) BMn10. Point 1, $CaHPO_4.2H_2O$ crystals; and point 2, $MnHPO_4(H_2O)_3$ crystals.

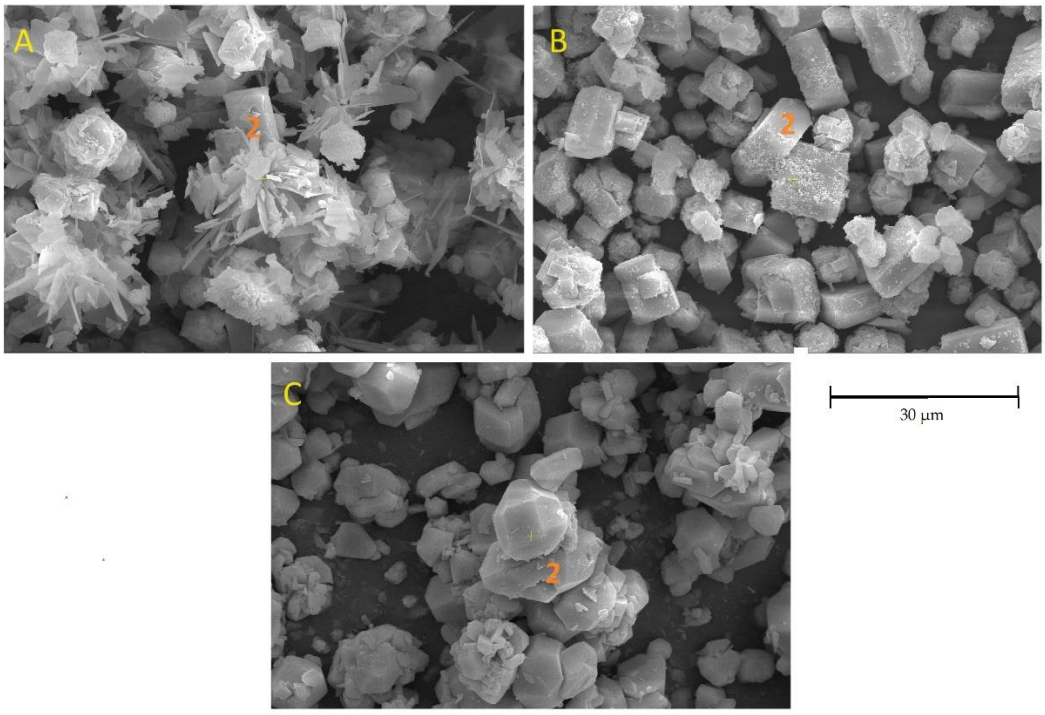

 doi:10.20944/preprints202408.2123.v1

Figure 6. SEM images of the $Ca_{1-x}Mn_xHPO_4{\cdot}nH_2O$ compounds with $MnHPO_4(H_2O)_3$ phase; (A) BMn6, (B) BMn8, and (C) BMn10; point 2: $MnHPO_4(H_2O)_3$ crystals.

3.2. FT-IR Spectrum of $Ca_{1-x}Mn_xHPO_4{\cdot}nH_2O$ Compounds

In Figure 7, the infrared spectral (FTIR) data for the $CaHPO_4{\cdot}2H_2O$, and $MnHPO_4(H_2O)_3$ phases are presented. The results of the FTIR analysis and the XRD investigation (Figure 2) were in agreement. The characteristic absorption bands of this phase [33,34] can be seen in the spectrum of $CaHPO_4{\cdot}2H_2O$ (BMn0), which was typical for this phase. The O-H stretching vibration caused by $CaHPO_4{\cdot}2H_2O$ [32] was the reason for the wide absorption peak, consisting of BMn0, BMn2, BMn4, BMn5, BMn6, BMn8, and BMn10, between 2400 cm^{-1} and 3600 cm^{-1}. The P-O-P asymmetric stretching vibration band was detected at 984 cm^{-1} due to P=O stretching vibrations, which led to the detection of an asymmetric stretching vibration band at 983 cm^{-1}. The other bands were detected at 654 and 569 cm^{-1}, and could be linked to the acid phosphates (H-O-)P=O [35]. The $CaHPO_4.2H_2O$ content in the samples led to a decrease in the intensity of another peak at 1643 cm^{-1}, which indicated the absence of water.

Due to the gradual increase in the Mn content in the basic solutions, from BMn2 up to BMn10, the produced compounds (BMn2, BMn4, BMn5, BMn6, BMn8, and BMn10) exhibited the growth of new peaks at 960 cm^{-1} and 548 cm^{-1}. These peaks corresponded to the P-O bending vibrations in $MnHPO_4(H_2O)_3$.

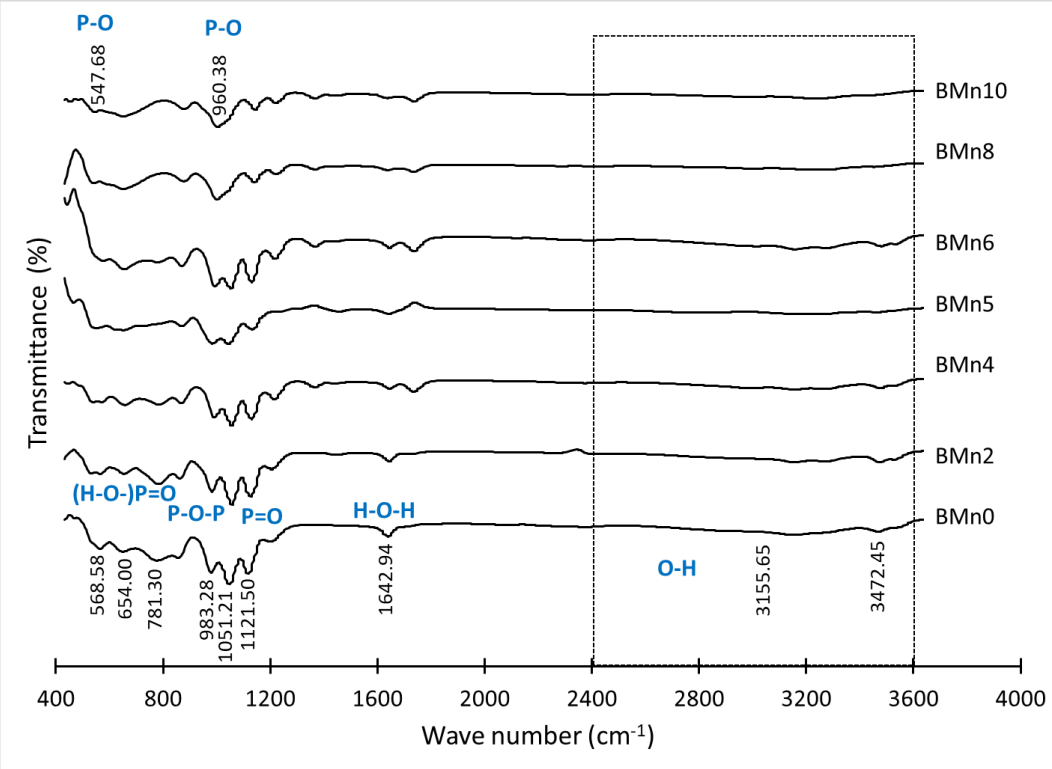

Figure 7. FT-IR spectra of $Ca_{1-x}Mn_xHPO_4{\cdot}nH_2O$ compounds.

3.3. Elemental Analysis of $Ca_{1-x}Mn_xHPO_4{\cdot}nH_2O$ Compounds

The prepared $Ca_{1-x}Mn_xHPO_4{\cdot}nH_2O$ compounds were subjected to an XPS analysis to determine the impact of the Mn/Ca molar ratio in the starting solutions on the chemical states of P, Mn, and Ca. The surface chemistry and characteristics in terms of the main elements (P, Mn, and Ca) of the prepared $Ca_{1-x}Mn_xHPO_4{\cdot}nH_2O$ compounds and the related results are shown in Figure 6.

 doi:10.20944/preprints202408.2123.v1

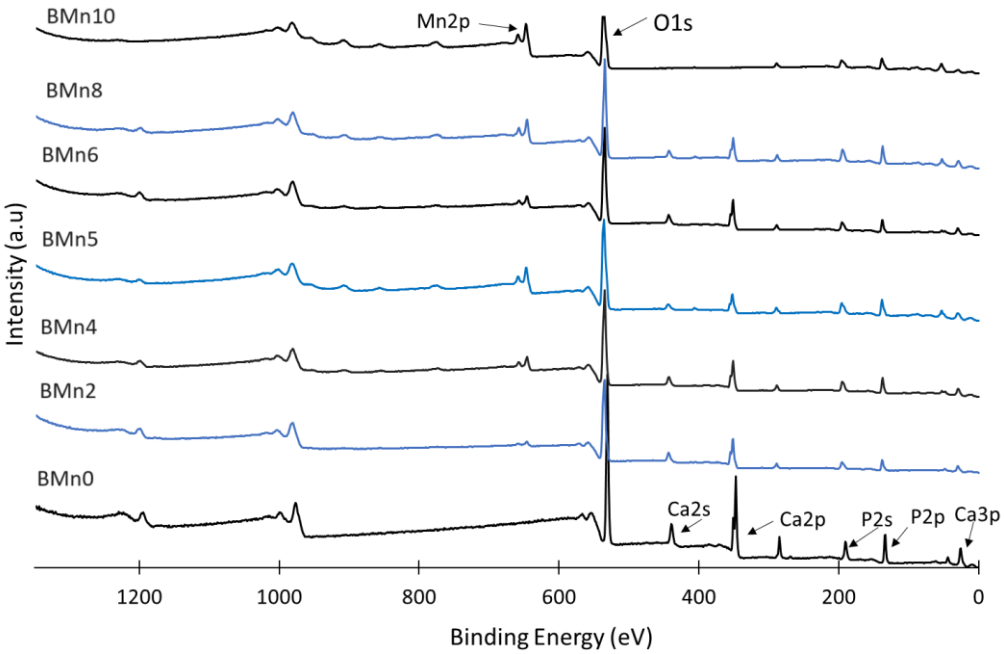

Figure 8. XPS spectra of the Ca1−xMnxHPO4·nH2O compounds.

Again, the Mn/Ca molar ratio was determined to influence the phase composition of the produced compound. The peaks relating to the Mn 2p orbital appeared in the XPS spectra of powders BMn2, BMn4, BMn5, BMn6, BMn8, and BMn10. The Mn concentrations increased up to 100% at the expense of the Ca concentrations; on the other hand, the intensity of the Ca 2s and Ca 2p peaks decreased in a manner closely related to the increase in the Mn/Ca molar ratio. The intensity of the peak corresponding to P 2s remained almost constant. This indicated that the concentrations of the P, Mn, and Ca peaks depended on the amount of Ca replacement with Mn in addition to the quantity of the synthesized powders (with higher Mn/Ca ratios).

The influence of the Mn/Ca molar ratio on the binding energies of Ca 2s, Mn 2p, and P 2s and the resultant XPS peaks are reported in Figure 9 (A–C), respectively. These results demonstrate that, in the case of the Mn/Ca 0.25 (BMn2) molar ratio, the binding energies of the P 2s and Ca 2s peaks rose from 438 eV to 443 eV and from 190 eV to 194 eV, respectively [7]. Meanwhile, the peaks corresponding to Ca 2p and Ca 2s no longer existed in the BMn10 compound. The binding energy corresponding to Mn 2p was observed to be 645-646 eV for those samples containing Mn (BMn2 to BMn10) [36].

The corresponding assessments of P 2s provided further evidence of how the Mn/Ca ratio rose to 1 (BMn5) and then decreased (BMn6), Figure 7C. The peaks corresponding to Ca 2s that appeared in BMn2–BMn6 indicated the precipitation of $CaHPO_4{\cdot}2H_2O$ alongside the $MnHPO_4(H_2O)_3$. However, these peaks disappeared with higher Mn/Ca molar ratios (BMn10) because of the formation of pure $MnHPO_4(H_2O)_3$. The XPS results showed that the binding energy in BMn5 was at the maximum for the three elements: Mn, Ca, and P.

Altogether, the XPS findings verified that, when the Mn/Ca molar ratio of the starting solution increased (BMn2–BMn6), a biphasic phosphate compound from $CaHPO_4{\cdot}2H_2O$ and $MnHPO_4(H_2O)_3$ was formed. However, to modify the crystal structure of the $Ca_{1-x}Mn_xHPO_4{\cdot}nH_2O$ compounds, it was sufficient to raise the binding energies of the Ca 2s and P 2s peaks. As the Mn intensity rose with a reduction in the Ca concentration, the level of supersaturation decreased (increased) with respect to $CaHPO_4{\cdot}2H_2O$. Consequently, a single-phase $MnHPO_4(H_2O)_3$ compound was obtained when a low percentage of Ca (under 40%) was available, as was the case with the BMn8 and BMn10 compounds.

The XPS findings confirmed that the presence of Mn was identified in compounds BMn2 to BMn10. Finally, the shifts in the peaks of Ca and P to higher positions as a result of adding Mn in the

 doi:10.20944/preprints202408.2123.v1

starting solutions (BMn2–BMn10) was an indication of changes to the areas surrounding these elements, caused by the precipitation of the new phase $MnHPO_4(H_2O)_3$.

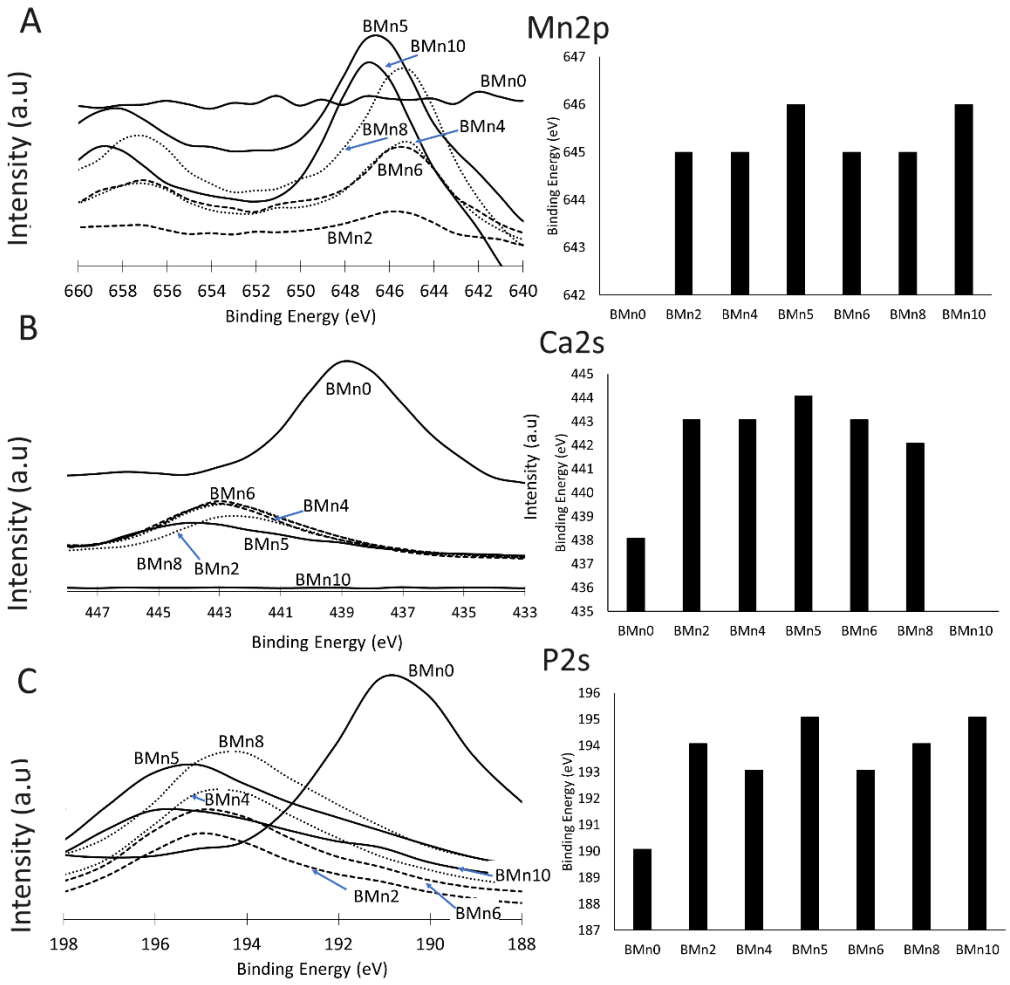

Figure 9. XPS analysis of the chemical state of (A) Mn 2p, (B) Ca 2s, and (C) P 2s orbitals in the $Ca_{1-x}Mn_xHPO_4{\cdot}nH_2O$ compounds.

3.4. Thermogravimetric Analysis (TGA)

In Figure 10, the results of the TGA analysis for the samples (BMn0 to BMn10) are presented. The crystal structure of $CaHPO_4.2H_2O$ was composed of compact analogous chains. These chains contained Ca ions, which were present as groups of six phosphate ions and two oxygen atoms that belonged to the chemically bonded water in $CaHPO_4{\cdot}2H_2O$ [36,37]. Furthermore, this was confirmed by two sharp peaks corresponding to the mass loss caused by increasing the temperature from 80 °C to 220 °C. $CaHPO_4{\cdot}2H_2O$ was identified by the two structural water molecules found in its lattice and the adsorbed water molecules on its surface [19,38]. The existing evidence suggests that part of the chemically bonded water was released when the $CaHPO_4{\cdot}2H_2O$ dehydrated and transformed to monetite ($CaHPO_4$) at ~220 °C. The dehydration of monetite ($CaHPO_4$) at ~400 °C resulted in the formation of calcium pyrophosphate ($Ca_2P_2O_7$) [39].

 doi:10.20944/preprints202408.2123.v1

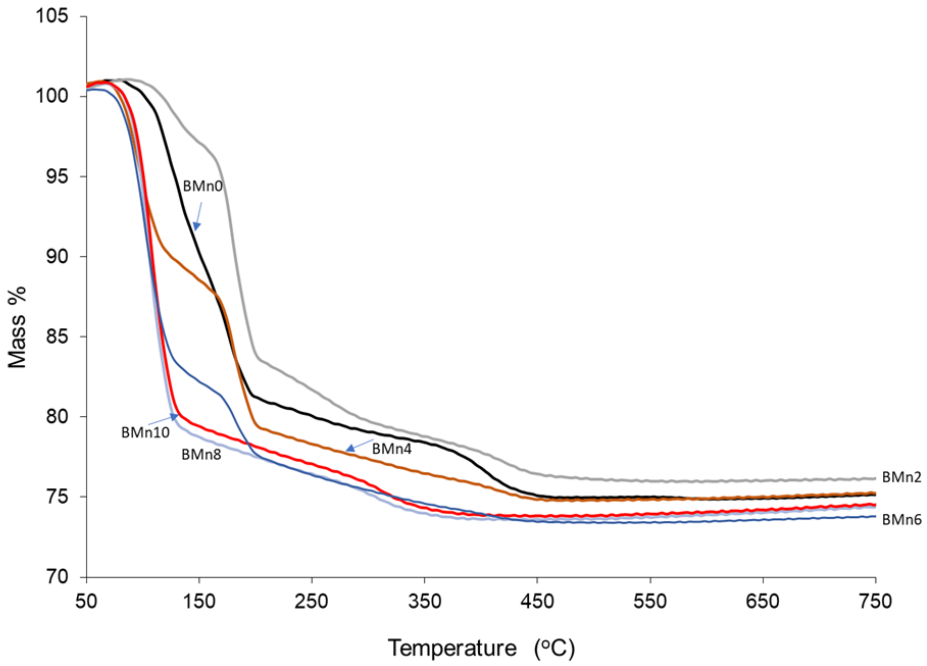

Figure 10. TG curves of the $Ca_{1-x}Mn_xHPO_4{\cdot}nH_2O$ compounds (BMn0–BMn10).

According to the results obtained in the present study, the mass loss of $CaHPO_4.2H_2O$ (BMn0) was roughly around 25 wt% when heated to 750 °C. This mass loss was larger than the hypothetical mass loss of 20.93 wt% [40]. The BMn2−BMn10 samples, with their increasingly higher Mn/Ca ratios, lost comparable masses, the percentage of which varied from 24% to 27%. The dehydration process of $CaHPO_4.2H_2O$ was based on Equation (1), while the calcination of $CaHPO_4$ and the subsequent transformation to calcium pyrophosphate is explained by Equation (2).

$$CaHPO_4 \cdot 2H_2O \rightarrow CaHPO_4 + 2H_2O \quad (1)$$

$$2CaHPO_4 \rightarrow Ca_2P_2O_7 + H_2O \quad (2)$$

Figure 11 shows the mass loss rate for the $Ca_{1-x}Mn_xHPO_4{\cdot}nH_2O$ compounds as a function of temperature. In an earlier study [19], as presented in Figure 9A−D, the mass loss peaks attributed to the two chemically bonded water molecules of $CaHPO_4.2H_2O$ were clearly visible below 200 °C. The thermal stability of the monophase $MnHPO_4(H2O)_3$ compound (BMn9 and BMn10) was studied (Figure 11). The mass loss below 130 °C was a result of releasing free, weakly adsorbed water, whereas a second weight loss around 300 °C was due to the dehydration of structural water. The gradual reduction in weight loss associated with $CaHPO_4$ at 400–420 °C was a strong indication of the increased magnesium phosphate content at the expense of $CaHPO_4.2H_2O$ in the resulting compounds, from BMn0 to BMn10. These findings are in agreement with the previous results obtained through XRD analysis (Figure 2).

Figure 11 illustrates how temperature affects the mass loss rate for the $Ca_{1-x}Mn_xHPO_4{\cdot}nH_2O$ compounds. As demonstrated in Figure 9A−D in an earlier study [19], the mass loss peaks associated with the two weakly and chemically bonded structural H_2O molecules of $CaHPO_4.2H_2O$ were readily visible at temperatures below 220 °C. This figure shows the results of an investigation on the heat loss of the monophase $MnHPO_4(H_2O)_3$ compound (BMn8 and BMn10). The release of free, weakly adsorbed water at lower temperatures was the cause of the mass loss, while the dehydration of structural water at higher temperatures was the cause of the second peak of mass loss at ~310 °C. The gradual reduction in weight loss associated with $CaHPO_4$, at 400–420 °C, was a strong indication of the increased $MnHPO_4(H_2O)_3$ content at the expense of $CaHPO_4.2H_2O$ in the synthesized compounds, from BMn0 to BMn10. These findings were consistent with the prior results obtained through XRD analysis (Figure 2).

 doi:10.20944/preprints202408.2123.v1

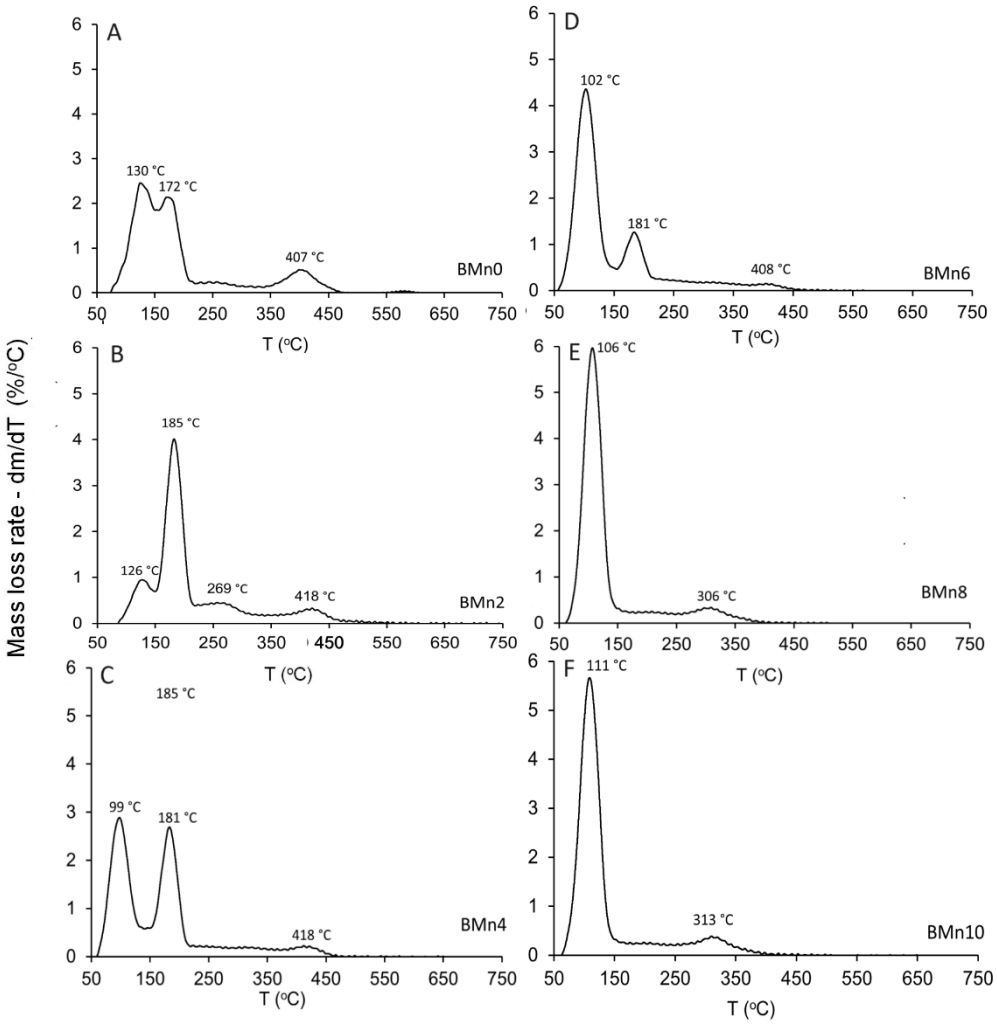

Figure 11. Mass loss rate as a function of temperature. (A) BMn0, (B) BMn2, (C) BMn4, (D) BMn6, (E) BMn8, and (F) BMn10.

4. Conclusions

The substitution and replacement of Ca ions with Mn ions in $CaHPO_4.2H_2O$ was investigated. As a result of this substitution/replacement, a series of $Ca_{1-x}Mn_xHPO_4{\cdot}nH_2O$ compounds, namely $CaHPO_4.2H_2O$ and $MnHPO_4(H_2O)_3$, were synthesized. Each compound was a single phase, or biphasic. The two phases observed as a result of the full-scale Ca replacement with Mn were as follows: $CaHPO_4{\cdot}2H_2O$, Mn-doped $CaHPO_4{\cdot}2H_2O$, biphasic $CaHPO_4.2H_2O$-$MnHPO_4(H_2O)_3$, Ca-doped $MnHPO_4(H_2O)_3$ and $MnHPO_4(H_2O)_3$. These findings show that, when the Mn/Ca molar ratio was below 0.25 (BMn2) in the starting calcium and phosphorus solutions, the Ca in $CaHPO_4.2H_2O$ was partially substituted by Mn. When increasing the Mn/Ca molar ratio, a biphasic $CaHPO_4.2H_2O$-$MnHPO_4(H_2O)_3$ compound was formed. The $MnHPO_4(H_2O)_3$ phase—which exhibited a orthorhombic crystal structure—formed at a Mn/Ca molar ratio above 0.25. When the Mn/Ca molar ratio progressively increased to 1.5 (whereby the solution's supersaturation level increased with respect to Mn), a biphasic compound of monoclinic $CaHPO_4.2H_2O$, and orthorhombic $MnHPO_4(H_2O)_3$ formed. Increasing the molar ratio of Mn vs. calcium to a level above 1.5 resulted in the precipitation of monophasic $MnHPO_4(H_2O)_3$ with an orthorhombic crystal structure. These results may be beneficial for the forthcoming production of precursors and biomaterials; these products can be synthesized with unique bespoke and structural characteristics. It has been suggested that, through changing the Mn/Ca molar ratio in the starting solution, a selection of geomorphologies and material components can be prepared.

 doi:10.20944/preprints202408.2123.v1

Author Contributions: Conceptualization, M. Ashaaer, M.A., and J.A..; Methodology, M. Ashaaer and F.A.; Software, M. Ashaaer; Validation, M. Ashaaer, J.A. and N.T.; Formal analysis, M. Ashaaer, M.A., and A.A.; Investigation, M. Ashaaer , M.A. , H.A., and N. T.; Resources, M. Ashaaer and F.A.; Data curation, M. Ashaaer, H.A., A.A., S.A., and F.A.; Writing—original draft preparation, M. Alshaaer, M.A., and J.A.; Writing—review and editing, M. Ashaaer and N. T.; Visualization, M. Ashaaer; Supervision, M. Ashaaer; Project administration, M. Ashaaer; Funding acquisition, M. Alshaaer. All authors have read and agreed to the published version of the manuscript.

Institutional Review Board Statement: N/A.

Acknowledgments: This study is supported via funding from Prince Sattam bin Abdulaziz University project number (PSAU/2024/R/1444).

Data Availability Statement: The data that support the findings of this study are available from the corresponding author, [M. Alshaaer], upon reasonable request.

Conflicts of Interest: The authors declare no conflicts of interest.

References

1. R. Khalifehzadeh and H. Arami, "Biodegradable calcium phosphate nanoparticles for cancer therapy," Advances in Colloid and Interface Science, vol. 279, 2020.
2. F. Wu, J. Wei, H. Guo, F. Chen, H. Hong and C. Liu, "Self-setting bioactive calcium-magnesium phosphate cement with high strength and degradability for bone regeneration," Acta Biomaterialia, vol. 4, no. 6, pp. 1873-1884, 2008.
3. M. Alshaaer, M. H. Kailani, H. Jafar, N. Ababneh and A. Awidi, "Physicochemical and Microstructural Characterization of Injectable Load-Bearing Calcium Phosphate Scaffold," Advances in Materials Science and Engineering, 2013.
4. I. Mert, S. Mandel and A. C. Tas, "Do cell culture solutions transform brushite (CaHP04 2H20) to octacalium phosphate (Ca8(HP04)2(P04)4 5H20)?," in Advances in Bioceramics and Porous Ceramics IV, R. Narayan and P. Colombo, Eds., Hoboken, New Jersey.: John Wiley & Sons, Inc., 2011, pp. 79-94.
5. M. Vallet-Regí, "Our contributions to applications of mesoporous silica nanoparticles," Acta Biomaterialia, vol. 137, pp. 44-52, 2022.
6. S. Sánchez-Salcedo, A. García, A. González-Jiménez and M. Vallet-Regí, "Antibacterial effect of 3D printed mesoporous bioactive glass scaffolds doped with metallic silver nanoparticles," Acta Biomaterialia, vol. 155, pp. 654-666, 2023.
7. M. Alshaaer, J. Al-Kafawein, A. Afify, N. Hamad, G. Saffarini and K. Issa, "Effect of Ca2+ Replacement with Cu2+ Ions in Brushite on the Phase Composition and Crystal Structure," Minerals, vol. 11, p. 1028, 2021.
8. V. Mouriño, J. Cattalini and A. Boccaccini, "Metallic ions as therapeutic agents in tissue engineering scaffolds: an overview of their biological applications and strategies for new developments," J R Soc Interface, vol. 9, no. 68, pp. 401-419, 2012.
9. S. Rosas, A. Ong, L. Buller, K. Sabeh, T. Law, M. Roche and V. Hernández, "Season of the year influences infection rates following total hip arthroplasty," World J. Orthop., vol. 8, no. 12, pp. 895-901, 2017.
10. S. Wei, J. Ma, L. Xu, X.-S. Gu and X.-L. Ma, "Biodegradable materials for bone defect repair," Military Medical Research, vol. 7, no. 54, 2020.
11. M. Alshaaer, M. H. Kailani, N. Ababneh, S. A. A. Mallouh, B. Sweileh and A. Awidi, "Fabrication of porous bioceramics for bone tissue applications using luffa cylindrical fibres (LCF) as template," Processing and Application of Ceramics , vol. 11, no. 1, p. 13–20, 2017.
12. H. Nosrati, D. Quang Svend Le, Zolfaghari, R. Emameh, Canillas, M. Perez and C. Eric Bünger, "Nucleation and growth of brushite crystals on the graphene sheets applicable in bone cement," Boletín de la Sociedad Española de Cerámica y Vidrio, 2020.
13. F. Tamimi, N. D. L., H. Eimar, Z. Sheikh, S. Komarova and J. Barralet, "The effect o fautoclaving on the physical and biological properties of dicalcium phosphate dihydrate bioceramics: Brushite vs. monetite," Acta Biomaterialia, vol. 8, no. 8, pp. 3161-3169, 2012.
14. K. Hurle, J. Oliveira, R. Reis, S. Pina and F. Goetz-Neunhoeffer, "Ion-doped Brushite Cements for Bone Regeneration," Acta Biomaterialia, 2021.
15. A. Dosen and R. F. Giese, "Thermal decomposition of brushite, CaHPO4·2H2O to monetite CaHPO4 and the formation of an amorphous phase," American Mineralogist, vol. 96, no. (2-3), p. 368–373, 2011.
16. N. H. Radwan, M. Nasr, R. A. Ishak, N. F. Abdeltawa and G. A. Awad, "Chitosan-calcium phosphate composite scaffolds for control of postoperative osteomyelitis: Fabrication, characterization, and in vitro–in vivo evaluation," Carbohydrate Polymers, vol. 244, p. 116482, 2020.
17. Z. Xue, Z. Wang, A. Sun, J. Huang, W. Wu, M. Chen, X. Hao, Z. Huang, X. Lin and S. Weng, "Rapid construction of polyetheretherketone (PEEK) biological implants incorporated with brushite

(CaHPO4·2H2O) and antibiotics for anti-infection and enhanced osseointegration," Materials Science and Engineering: C, vol. 111, 2020.
18. B.-Q. Lu, T. Willhammar, B.-B. Sun, N. Hedin, J. D. Gale and D. Gebauer, "Introducing the crystalline phase of dicalcium phosphate monohydrate," Nat Commun, vol. 11, p. 1546, 2020.
19. L. Tortet, J. R. Gavarri and G. Nihoul, "Study of Protonic Mobility in CaHPO4 · 2H2O (Brushite) and CaHPO4 (Monetite) by Infrared Spectroscopy and Neutron Scattering," Journal of Solid State Chemistry, vol. 132, pp. 6-16, 1997.
20. N. Matsumoto, K. Sato, K. Yoshida, K. Hashimoto and Y. Toda, "Preparation and characterization of beta-tricalcium phosphate co-doped with monovalent and divalent antibacterial metal ions," Acta Biomater., vol. 5, pp. 3157-3164, 2009.
21. I. Mayer, O. Jacobsohn, T. Niazov, J. Werckmann, M. Iliescu, M. Richard-Plouet, O. Burghaus and D. Reinen, "Manganese in Precipitated Hydroxyapatites," European journal of inorganic chemistry, vol. 2003, p. 1445−1451, 2003.
22. E. Boanini, F. Silingardi, M. Gazzano and A. Bigi, "Synthesis and Hydrolysis of Brushite (DCPD): The Role of Ionic Substitution," Crystal Growth & Design, vol. 21, p. 1689−1697, 2021.
23. H. E. L. Madsen, "influence of foreign metal ions on crystal growth and morphology of brushite (CaHPO4, 2H2O) and its transformation to octacalcium phosphate and apatite," Journal of Crystal Growth, vol. 310, no. 10, pp. 2602-2612, 2008.
24. D. Griesiute, E. Garskaite, A. Antuzevics, V. Klimavicius, V. Balevicius, A. Zarkov, A. Katelnikovas, D. Sandberg and A. Kareiva, "Synthesis, structural and luminescent properties of Mn-doped calcium pyrophosphate (Ca2P2O7) polymorphs," Scientific Reports, vol. 12, p. 7116, 2022.
25. S. B. Patil, A. Jena and P. Bhargava, "Influence of Ethanol Amount During Washing on Deagglomeration of Co-Precipitated Calcined Nanocrystalline 3YSZ Powders," International Journal of Applied Ceramic Technology, 2012.
26. R. H. Piva, D. H. Piva, J. Pierri, O. R. K. Montedo and M. R. Morelli, "Azeotropic distillation, ethanol washing, and freeze drying on coprecipitated gels for production of high surface area 3Y–TZP and 8YSZ powders: A comparative study," Ceramics International, vol. 41, pp. 14148-14156, 2015.
27. M. Alshaaer, A. Afify, M. Moustapha, N. Hamad, G. Hammouda and F. Rocha, "Effects of the full-scale substitution of strontium for calcium on the microstructure of brushite: (CaxSr1–x)HPO4.nH2O system," Clay Minerals, vol. 55, no. 4, pp. 366-374, 2020.
28. Schofield P. F., Knight K. S., van der Houwen J. A. M., Valsami-Jones E, "The role of hydrogen bonding in the thermal expansion and dehydrationof brushite, di-calcium phosphate dihydrateSample: T = 4.2 K", Physics and Chemistry of Minerals 31, 606-624 (2004)
29. Jin K, Park J, Lee J, Yang KD, Pradhan GK, Sim U, Jeong D, Jang HL, Park S, Kim D, Sung NE, Kim SH, Han S, Nam KT. Hydrated manganese(II) phosphate ($Mn_3(PO_4)_2·3H_2O$) as a water oxidation catalyst. J Am Chem Soc. 2014 May 21;136(20):7435-43. doi: 10.1021/ja5026529. Epub 2014 May 7. PMID: 24758237.
30. F. Abdulaziz, K. Issa, M. Alyami, S. Alotibi, A. Alanazi, T. Taha, A. Saad, G. Hammouda, N. Hamad and M. Alshaaer, "Preparation and Characterization of Mono- and Biphasic Ca1−xAgxHPO4·nH2O Compounds for Biomedical Applications," Biomimetics, vol. 8, p. 547, 2023.
31. S. Wang, R. Zhao, S. Yao, B. Li, R. Liu, L. Hu, A. Zhang, R. Yang, X. Liu, Z. Fu, D. Wang, Z. Yang and Y.-M. Yan, "Stretching the c-axis of the Mn3O4 lattice with broadened ion transfer channels for enhanced Na-ion storage," Journal of Materials Chemistry A, vol. 9, no. 41, pp. 23506-23514, 2021.
32. S. S. Alotibi and M. Alshaaer, "The Effect of Full-Scale Exchange of Ca2+ with Co2+ Ions on the Crystal Structure and Phase Composition of CaHPO4·2H2O," Crystals, vol. 13, no. 6, p. 941, 2023.
33. L. Tortet, J. R. Gavarri, G. Nihoul and A. J. Dianoux, "Study of Protonic Mobility in CaHPO4·2H2O (Brushite) and CaHPO4 (Monetite) by Infrared Spectroscopy and Neutron Scattering," J. Solid State Chem., vol. 132, p. 6– 16, 1997.
34. A. Hirsch, I. Azuri, L. Addadi, S. Weiner, K. Yang, S. Curtarolo and L. Kronik, "Infrared Absorption Spectrum of Brushite from First Principles," Chem. Mater. , vol. 26, p. 2934– 2942, 2014.
35. K. K. C. Rajendran, "Growth and Characterization of Calcium Hydrogen Phosphate Dihydrate Crystals from Single Dif-fusion Gel Technique," Cryst. Res. Technol, vol. 45, no. 9, pp. 939- 945, 2010.
36. Wang, T., Li, Z. Effects of MnO_2 addition on the structure and electrical properties of PIN-PZN-PT ceramics with MPB composition. *J Mater Sci: Mater Electron* **31**, 22740–22748 (2020). https://doi.org/10.1007/s10854-020-04798-2
37. M. Alshaaer, H. Cuypers, H. Rahier and J. Wastiels, "Production of monetite-based Inorganic Phosphate Cement (M-IPC) using hydrothermal post curing (HTPC)," Cement and Concrete Research, vol. 41, p. 30–37, 2011.
38. Dosen, Anja and Giese, Rossman F.. "Thermal decomposition of brushite, CaHPO4·2H2O to monetite CaHPO4 and the formation of an amorphous phase" American Mineralogist, vol. 96, no. 2-3, 2011, pp. 368-373. https://doi.org/10.2138/am.2011.3544

 doi:10.20944/preprints202408.2123.v1

39. M. Alshaaer, H. Cuypers, G. Mosselmans, H. Rahier and J. Wastiels, "Evaluation of a low temperature hardening Inorganic Phosphate Cement for high-temperature applications," Cement and Concrete Research, vol. 41, p. 38–45, 2011.
40. R. L. Frost and S. J. Palmer, "Thermal stability of the 'cave' mineral brushite CaHPO4·2H2O – Mechanism of formation and decomposition," Thermochimica Acta, vol. 521, no. 1-2, pp. 14-17, 2011.